La mer 30: 239–250, 1992
Société franco-japonaise d'océanographie, Tokyo

Numerical simulation of seasonal cycle of world ocean general circulations

X. -H. ZHANG*, N. BAO* and W. -Q. WANG*

Abstract: A revised version of the IAP four-layer world ocean general circulation model is presented. The new version has been integrated for 180 years for an annual mean simulation and for subsequent 40 years for a seasonal cycle simulation. Analysis of the annual mean and monthly mean results including temperature, salinity, sea surface elevation, currents and energy indicates that the upper two layers of the model have already reached an equilibrium, while the lower two layers have not. The simulated sea surface temperature has been remarkably improved compared with the previous results due to the use of Haney-type heat flux formulation at the sea surface. The annual mean and seasonal salinity have also been simulated with reasonable accuracy by using a buoyancy equation and a simple sea surface buoyancy flux condition. One of the important characteristics of the model's available surface potential energy defined by ZENG (1983) is that its value over the southern ocean is greater than that over the northern ocean reflecting a strong gradient in the Antarctic Circumpolar Current. The strongest signal of seasonal variability for the surface current has been found in the Somali Current just as pointed out by HAN (1984). It has also been found that the seasonal forcing penetrates into the model's subsurface layer only in the Indian Ocean.

1. Introduction

The first multi-layer version of the IAP (Institute of Atmospheric Physics, Chinese Academy of Sciences) ocean general circulation model (OGCM) was presented in 1988 (ZHANG and ZENG, 1988; ZHANG and LIANG, 1989). The model was designed based on a set of full primitive equations without the "rigid-lid" approximation (ZENG, 1983). In the vertical, a set of "standard" stratification parameters were introduced into the governing equations of the model, and all the thermodynamic variables including temperature, salinity, density and pressure were replaced by their departures from the "standards" (ZENG, 1983; ZENG *et al.*, 1991). The model's geography was fairly realistic except that the Arctic Sea was not included in the model and that the northern boundary of the North Atlantic was closed. The so-called C-grid (ARAKAWA *et al.*, 1977) with the grid size of 4° in latitude and 5° in longitude was used in the model's horizontal discretization. The bottom topography of the model was highly smoothed with the maximum depth of 3200 m and the minimum depth of 1000 m to adapt to a terrain-following coordinate. In fact, the model used the "sigma"-coordinate in the vertical (ZENG, 1983) and had four layers with the variable thickness. The maximum depths of the four layers were 100 m, 500 m, 1,500 m and 3,200 m, respectively. The spatial finite-difference schemes of the model were designed to conserve the "available" energy (ZENG and ZHANG, 1987) defined as the sum of kinetic energy (KE), available potential energy (APE) and available surface potential energy (ASPE), which is related to the sea surface fluctuation in an OGCM providing that the source and sink terms of the model are in a perfect equilibrium.

The model was integrated by using an asynchronous technique based on the "flexible" coefficients (ZENG *et al.*, 1982) for more than 20

* Laboratory of Numerical Modelling for Atmospheric Sciences and Geophysical Fluid Dynamics, Institute of Atmospheric Physics, Chinese Academy of Sciences, Beijing, 100080 China

years for the advection terms and more than 60 yeard for the vertical thermal diffusion in response to the observed annual mean atmospheric forcing including wind stress, air pressure and air temperature at the sea level. The preliminary success of the model in reproducing qualitatively many aspects of large-scale features of the annual mean world ocean general circulation indicates that the fundamental design of the IAP OGCM is reasonable and its use is feasible in practice.

While the preliminary success is encouraging, there is still a lot to be done, e.g., the inclusion of the salinity variation in the model's integration. There are some problems to be solved, e.g., the simulated sea surface temperature in the tropical western Pacific is 2–3℃ lower than the observation. In addition, the integration is far from being long enough for the model to reach a quasi-steady state and to be validated confidently. Therefore, in the past two years, continuous efforts have been made on the model's improvement by IAP, and a revised version of the model is presented now. The new model has been integrated for 180 years with the observed annual mean atmospheric forcing and for subsequent 40 years with the seasonal atmospheric forcing. The results show that significant improvements have been achieved.

In this paper, the new version of the IAP world OGCM and its performance will be depicted. The new version itself will be briefly described in contrast with the old version in Section 2. Some results of the annual mean simulation especially those improved aspects compared with the previous results will be shown in Section 3. A somewhat detailed portrayal of the simulated seasonal cycle of ocean general circulation will be given in Section 4.

2. Model description

The new version of the IAP world OGCM is different from the original version (ZHANG and LIANG, 1989) mainly in the following aspects.

a) To include the variation of salinity in the model's integration, we introduce the Archimedean buoyancy into the model defined as $g' = -g\rho'/\rho_0$, where $\rho' = \rho - \bar{\rho}$ is the difference between the density of the sea water, ρ, and its "standard" vertical profile $\bar{\rho} = \bar{\rho}(z)$. The $\bar{\rho}(z)$ is obtained by using the "standard" vertical temperature profile, $\bar{T} = \bar{T}(z)$, and salinity profile, $\bar{S} = \bar{S}(z)$, in the state equation of the sea water (Eckart, 1958). Let $T' = T - \bar{T}$ and $S' = S - \bar{S}$, then a linearized version of the state equation of sea water, which represents the relationship among the perturbed density ρ', perturbed temperature, T' and perturbed salinity S', can be derived, and accordingly the Archimedean buoyancy is expressed as

$$g' = g(\alpha_T T' - \alpha_S S') \tag{1}$$

where α_T is the thermal expansion coefficient and α_S is the density-salinity coefficient, both of them being functions of the depth z.

Thus S', one of the prognostic variables of the original model, is replaced by g' in the new version, and correspondingly the perturbed salinity equation and the boundary condition at the surface are replaced by a buoyancy equation and a buoyancy condition which are directly derived by using the equations and boundary conditions for the perturbed temperature and salinity (ZHANG and BAO, 1990). The perturbed salinity, one of the diagnostic variables of the new model, is calulated by using Eq. (1) while g' and T' are predicted.

The APE is now defined as

$$APE = \frac{\rho_0}{2} \iiint \left(\frac{g'}{N}\right)^2 dz\, ds \tag{2}$$

where N is the Brunt-Väisälä frequency determined by using the "standard" stratifications of temperature and salinity, and $N^2 > 0$ is true everywhere for large-scale oceanic circulations. With S', one of the prognostic variables in the original model, however, we have to use an alternative expression for APE, i.e.,

$$APE = \frac{\rho_0 g}{2} \iiint \left(\frac{\alpha_T}{\Gamma_T}(T')^2 + \frac{\alpha_S}{\Gamma_S}(S')^2\right) dz\, ds \tag{3}$$

where $\Gamma_T = d\bar{T}/dz$ and $\Gamma_S = d\bar{S}/dz$. The problem is that Γ_S decreases with depth within the thermocline (e. g., LEVITUS, 1982), thereby making the APE not definable in terms of Eq. (3). That is why the Archimedean buoyancy, g', rather than the perturbed salinity, S', is used

as a prognostic variable in the new version.

The "standard" stratifications of temperature and salinity in the original model were taken from the work of BRYAN and COX (1972), which represents the observed medium values of temperature and salinity in the world ocean rather than the globally averaged ones. As a result, the "standard" sea surface temperature is only 15℃ which is 3℃ lower than the observed global annual-mean SST. In the new model, therefore, the observed global annual-mean temperature and salinity (LEVITUS, 1982) are taken as the "standard" ones instead of the original ones. Meanwhile, a linearized state equation of sea water relating the perturbed density, temperature and salinity is directly derived by using the Eckart formula rather than the Bryan-Cox formula.

b) The heat flux at the air-sea interface, as the upper boundary condition for the thermodynamic equation, is computed for 150 years by using the Newtonian cooling formulation which is the same as that used in the original version. The formulation can be written as

$$F=\rho_0 C_p \mu_T (T_a - T_1) \tag{4}$$

where T_a is the observed sea level air temperature, T_1 represents the simulated ocean surface layer temperature, and μ_T^{-1} represents the rate of thermal penetration through the surface with a value of 2 day m^{-1}.

After 150 years, a Haney-type formula such as

$$F=D(T_A - T_1) \tag{5}$$

is used to replace Eq. (4). Here, D is the heat transfer coefficient and $T_A = T_a + Q_l/D$ represents the "apparent" atmospheric equilibrium temperature, where Q_l depends on the net downward solar radiation flux, downward atmospheric long wave radiation flux, and latent heat flux. D and Q_l are computed as functions of climatological atmospheric parameters obtained from various sources (HAN, 1984).

In contrast to Eq. (4), Eq. (5) gives $\mu_T^{-1} = D/\rho_0 C_p$, which is a variable parameter ranging from 0.8 to 1.9 day m^{-1}. Further, Q_l/D representing the difference between the "apparent" air temperature, T_A, and the real air temperature, T_a, is significant in the tropical areas, which is a crucial factor for the improvement of the simulated tropical SST.

c) One of the most important parameters in the OGCMs is the vertical thermal diffusivity which the e-folding scale depth of the thermocline is almost proportional to (BRYAN, 1987). Unfortunately, the vertical diffusivity is one of the most uncertain parameters in the OGCMs due to the lack of the observational data necessary for its determination. The constant diffusivity ($10^{-4} m^2 s^{-1}$) used in the original model does not seem to be a reasonable choice because the solution to the corresponding vertical thermal diffusion equation will approach a vertically homogeneous state while the adiabatic bottom boundary condition is used.

In the new version, a depth-dependent vertical thermal diffusivity defined as (BRYAN and LEWIS, 1979)

$$k=k(z)=10^{-4}[0.8+(1.05/\pi)\tan^{-1}\{4.5\,(z-2500)/1000\}] \tag{6}$$

is used instead of a constant one. The value given by Eq. (6) is about $0.3\times10^{-4} m^2 s^{-1}$ within the surface layer and about $1.3\times10^{-4} m^2 s^{-1}$ near the bottom, which is compatible with observational evidences (ROOTH *et al.*, 1972; MUNK, 1966). Although the vertical diffusivity representation may not be suitable everywhere, we find that its smallness within the upper layer is favorable to the heat accumulation in the upper ocean (BAO and ZHANG, 1991).

d) The C-grid and the relevant finite-difference schemes used in the original version are substituted by the B-grid and the corresponding available energy-conserving finite-difference schemes (ZENG and ZHANG, 1987) in the new version in order to reduce the small scale noise excited more easily in full primitive equation model than in model with the "rigid-lid" approximation. Comparative experiments with the two kinds of grid show that the B-grid is more favorable to suppress the noise between the two adjacent grids than the C-grid especially around the Antarctica. The reason for this is that the B-grid and the conventional horizontal diffusion scheme are complementary to one another in respect to controlling computational noise as pointed out by BATTEEN and HAN

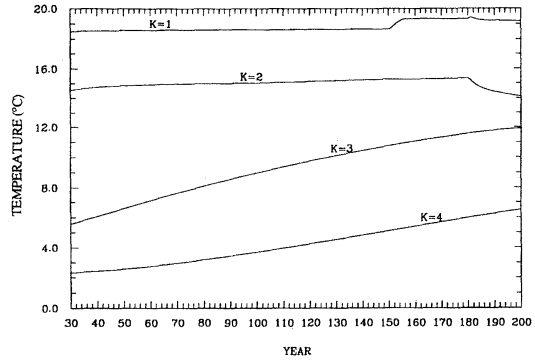

Fig. 1. Computed global annual-mean temperature during the years 30–200 of integration.

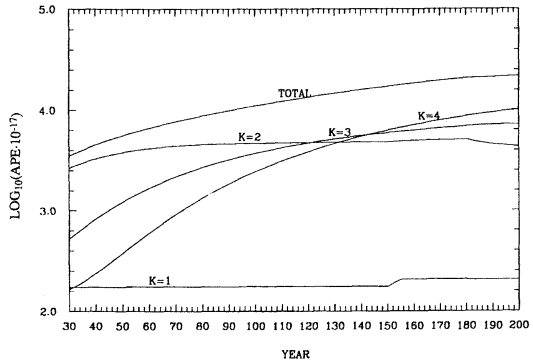

Fig. 2. The rate of the computed APE increase for the years 30–200 of integration.

(1981).

e) To decrease the horizontal variability of the layer thickness, the minimum depth near the coastal region is increased up to 1600 m which is half the maximum depth in the new version. Furthermore, the maximum thickness of the surface layer is now reduced to 50 m in order to lower its thermal inertia.

3. Improved annual mean simulation

First, the model was integrated for 180 years in response to the observed annual mean sea level wind stress (HAN *et al.*, 1981), sea level air temperature and pressure (ESBENSEN *et al.*, 1981) and sea surface salinity (LEVITUS, 1982). The integration started from a motionless initial state, of which the sea surface was flat and the departures of temperature and salinity were zero. To establish a benchmark solutions which may be used in evaluating various time integration techniques in the future, the "leap-frog" method with a time step of 10 minutes combined with an Euler-forward scheme employed once a month is used in the present model. In addition, a 9-point smoother is used once every 5 years for the current velocity components and every year for the temperature and salinity to suppress the computational noise of the prognostic variables. Also, the horizontal viscosity coefficient, A_m, is increased to $1.2\times10^6 m^2 s^{-1}$ from its original value of $0.8\times10^6 m^2 s^{-1}$.

As mentioned in Section 2, the sea surface heat flux was calculated by using Eq. (4) with $\mu_T=0.5$ m day^{-1} for 150 years and after that by using Eq. (5) with D and T_A being computed from the observed annual mean atmospheric data and some empirical parameters (HAN, 1984). Such a change has been proven very important for improving the simulated surface layer temperature as shown in Fig. 1, in which the maximum undergoes a rapid increase between the year 150 and 156. Comparing the horizontal distributions of the temperature for the year 150 (Fig. 3b) and the year 163 (Fig. 3c) we find that the latter is much closer to the observation (Fig. 3a) than the former, especially in the warm pool region of the western Pacific.

It can be shown from Fig. 1 that the global annual-mean temperatures of the first and second layers have already reached the equilibrium by the end of the integration. This can also be shown in the temporal evolution of the global annual-mean salinity for the upper two layers, the annual mean ASPE and of the annual mean KE (not shown here). On the other hand, the same is not true for the two lower-layer temperatures and salinities, which continuously increase in the course of the integration reflecting a rather significant trend of the annual mean APE (Fig. 2). We speculate that this phenomenon is due to the lack of the formation of the bottom water in this model.

Fig. 4b shows the simulated annual mean surface salinity, which is in good agreement with the observation (Fig. 4a). Such an agreement comes easily from the use of the observed salinity data rather than the evaporation, precipitation and runoff data in the computation of the fresh water flux at the sea surface (ZHANG and BAO, 1990).

One major feature of the IAP OGCM is the relaxation of the "rigid-lid" assumption. There-

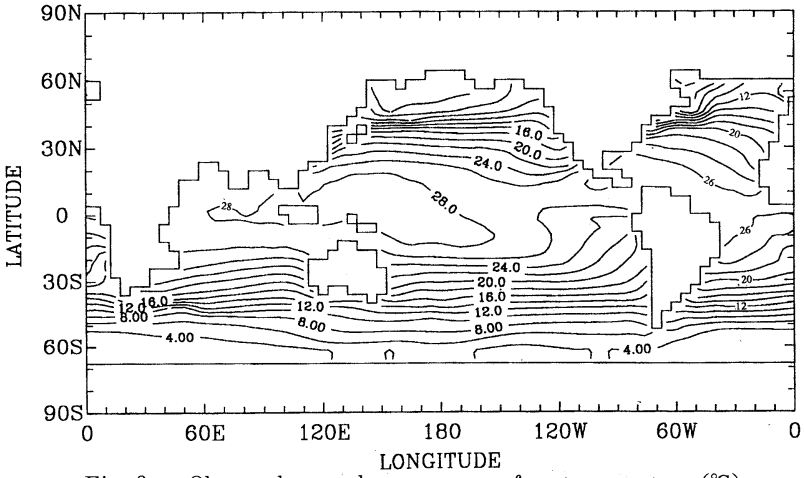

Fig. 3a. Observed annual mean sea surface temperature (℃).

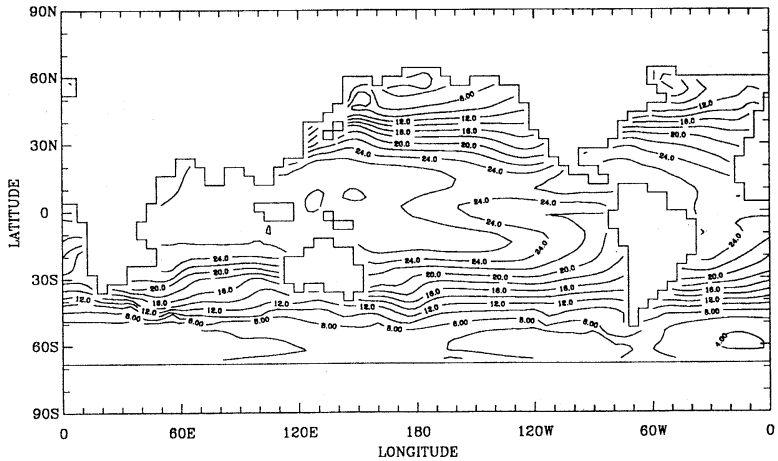

Fig. 3b. Simulated sea surface temperature (℃) in the year 150.

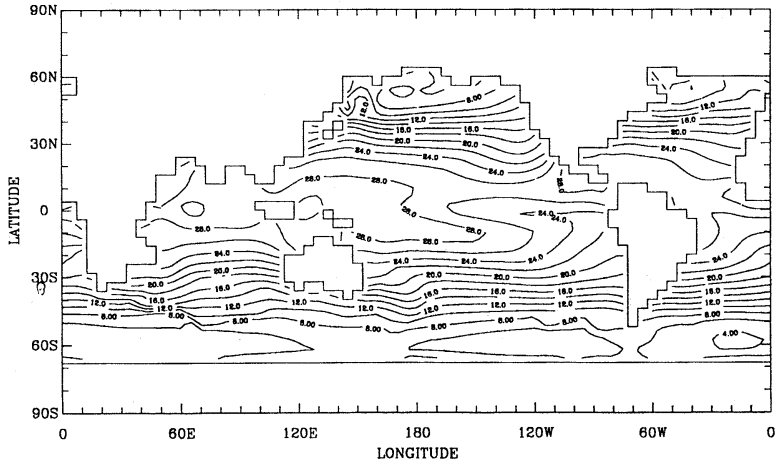

Fig. 3c. Simulated sea surface temperature (℃) in the year 163.

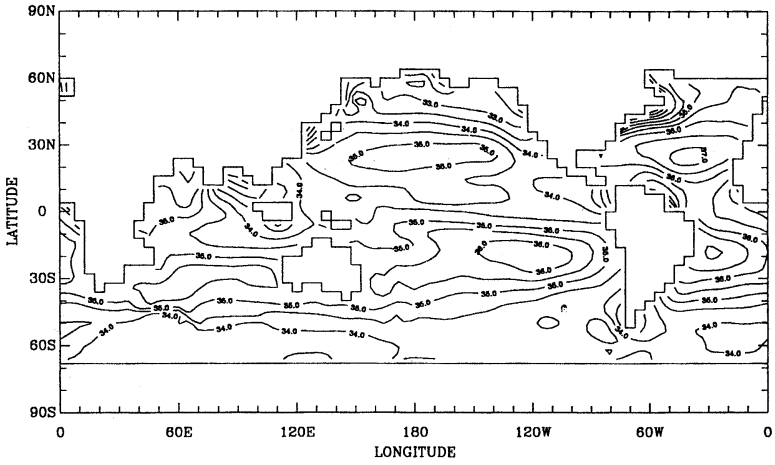

Fig. 4a. Observed annual mean surface layer salinity (g kg^{-1}) (from LEVITUS, 1982).

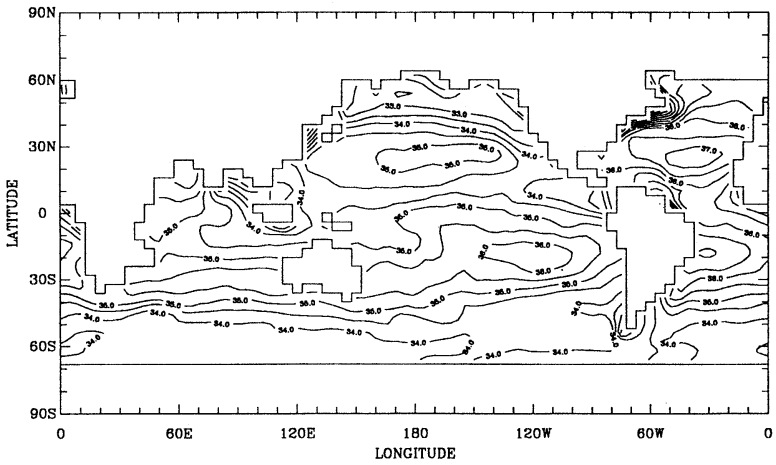

Fig. 4b. Simulated annual mean surface layer salinity (g kg^{-1}) in the year 180.

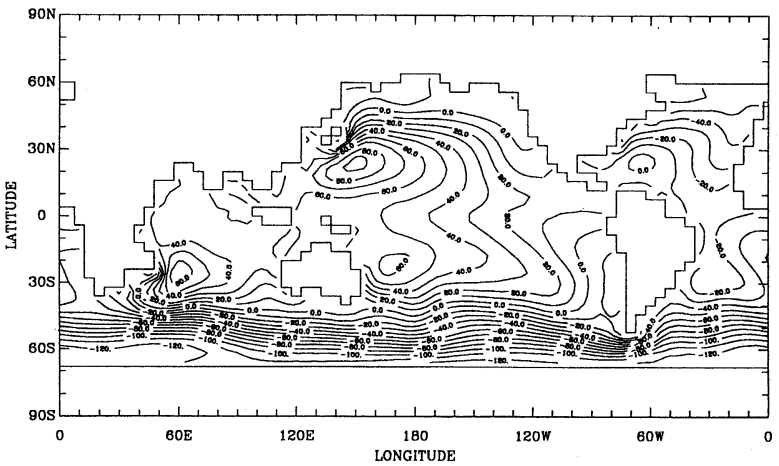

Fig. 5. Simulated sea surface elevation (cm) in the year 180.

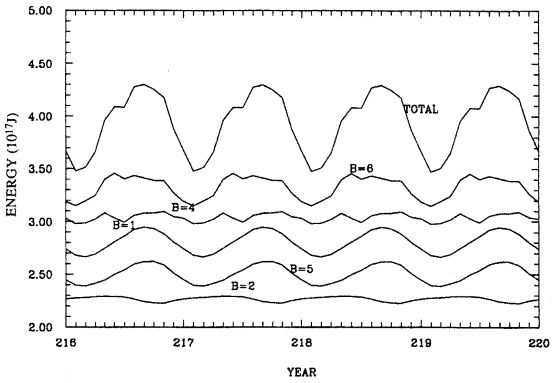

Fig. 6. Monthly mean available surface potential energy in five basins.
B=1 - North Pacific (+ 2.00); B=5 - South Atlantic (+ 1.75);
B=4 - South Pacific (+ 2.00); B=6 - Indian Ocean (+ 2.25).
B=2 - North Atlantic (+ 2.00);

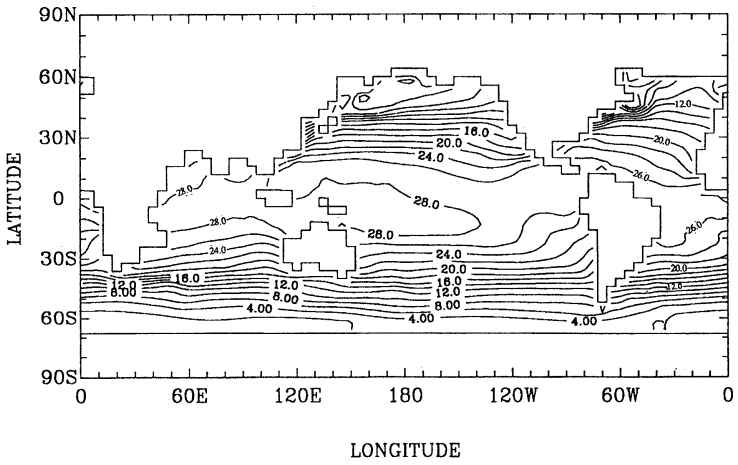

Fig. 7a. Observed monthly mean SST (℃) in March (from ESBENSEN *et al.*, 1981).

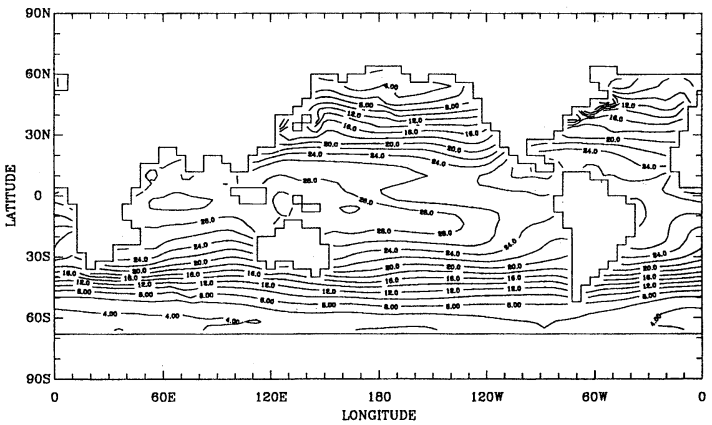

Fig. 7b. Simulated monthly mean surface layer temperature (℃) in March (year 200).

fore, the sea surface elevation is one of the model's prognostic variables. Fig. 5 shows the simulated annual mean sea surface elevation for the year 180, in which the highest region in the western Pacific with a central value greater than 90 cm is much closer to the observed result (WYRTKI, 1975) than that simulated by the original model (Fig. 12 of ZHANG and LIANG, 1989). Meanwhile, the simulated poleward gradient around the Antarctica is much stronger than in the original model. It implies that the Antarctic Circumpolar Current, which was poorly described in the old model, has been improved remarkably in the present simulation.

4. Some results of seasonal cycle simulation

After 180 years of simulation with the annual mean forcing the model has been integrated subsequently for another 40 years with the observed seasonal atmospheric forcing. The sea level wind stress, air pressure, T_A, D and sea surface salinity are updated at the end of each day by the linear interpolation of the consecutive monthly mean values (HAN *et al.*, 1981; ESBENSEN *et al.*, 1981; LEVITUS, 1982). The model's climate undergoes an adjustment during the first few years due to the change in forcing conditions from steady to periodic. However, a periodical solution is reached soon after except for some lower

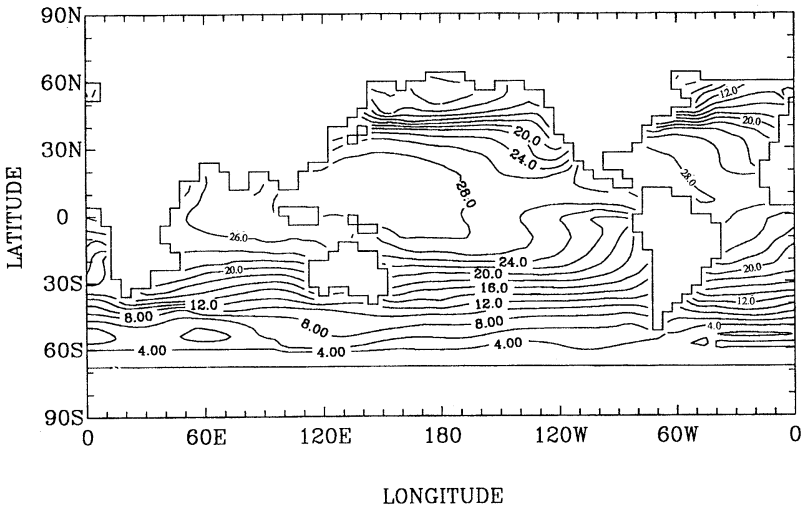

Fig. 8a. Observed monthly mean SST (℃) in September (from ESBENSEN *et al.*, 1981).

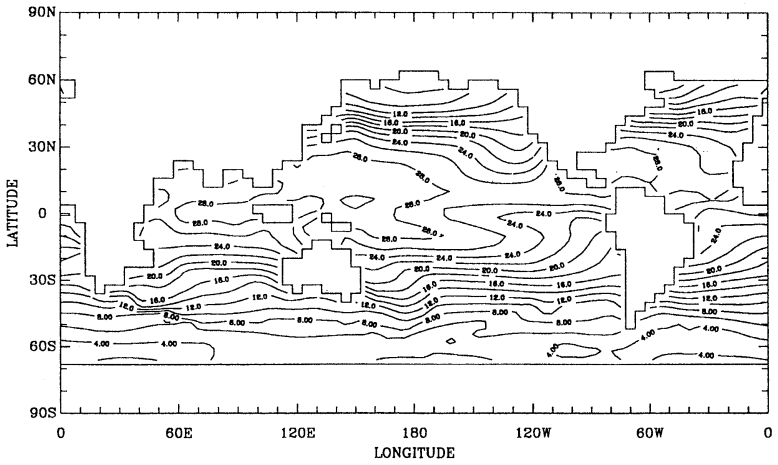

Fig. 8b. Simulated monthly mean surface layer temperature (℃) in September (year 200).

layer variables. In the following, the model's seasonal cycles will be depicted by using the consecutive monthly mean values of some variables during the last 20 years (years 200–220).

Fig. 6 shows the variation of monthly mean ASPE during the last 4 years (years 216–220) defined as

$$ASPE = \frac{\rho_0}{2g} \int (gz_0)^2 ds \qquad (7)$$

where z_0 is the sea surface elevation with its average value being zero. Some perfect periodical oscillations can be found from not only the global ASPE but also the basin-based ASPE. One of the important features for the basin-based ASPE is that its value in the South Pacific (B=4) is greater than in the North Pacific (B=1) and so is in the Atlantic (B=5 and B=2) reflecting the strong sea surface slope around the Antarctica (Fig. 5). However, the seasonal cycle of the ASPE in the South Pacific is weaker than that in the North Pacific, which is opposite to the contrast in the seasonal cycle of the ASPE between the South and North Atlantic.

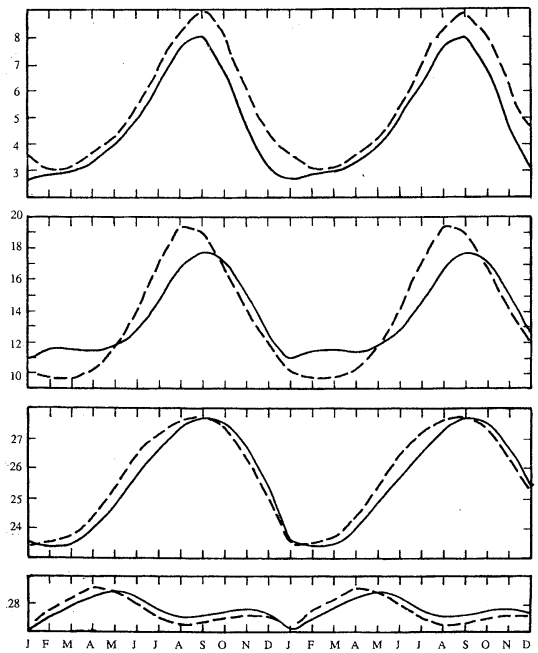

Fig. 9. Simulated (solid line) and observed (dashed line) zonal mean SSTs (℃) at 2°N, 22°N, 42°N and 62°N (from the bottom to the top).

Figs. 7a, b are the observed and simulated SSTs in March. A good agreement is in the warm pool region of the western Pacific. On the other hand, the simulated maximum SST in the equatorial Indian Ocean, which is over 30℃, does not seem to be realistic. Besides, the simulated SSTs over the equatorial central and eastern Pacific regions are more than 1℃ lower than the observation, which may be related to the overestimated cold water upwelling by the model. Similar features are also found in the simulated SST in September (Fig. 8) with the contrast between the warm water in the western Pacific and the cold water in the eastern Pacific being sharper than in March.

The zonal averages of both the simulated and observed temperatures are computed at each of the four latitudes 2° N, 22° N, 42° N and 62° N, and the results are shown as a function of time in Fig. 9. Some typical characteristics such as the large seasonal variability in the middle and high latitudes, and the semi-annual variation with relatively small amplitude near the equator (HAN, 1984) are reproduced. In general, the simulated results are in good agreement with the observations despite some small discrepancies in the amplitude and phase (e.g., the simulated annual amplitude at 42° N is 2℃ lower and lags the observation by 1 month).

The simulated surface currents for January and July are shown in Figs. 10a and 10b, respectively. Remarkable seasonal differences are found by comparing the simulated major current systems such as the Equatorial Current, Gulf Stream, Kuroshio, Somali Current, and the Australia Current for January and July. The sharpest seasonal contrast between January and July seems to be in the Indian Ocean. For instance, as shown in Fig. 11, the seasonal amplitudes of the maximum northward and eastward currents in the Indian Ocean are 13 cm s^{-1} and 18 cm s^{-1}, respectively, by the Somali Current just as pointed by HAN based on the results of OSU OGCM (HAN, 1984). The corresponding values in the North Pacific are only 5 cm s^{-1} and 4 cm s^{-1}, respectively (Fig. 12). Furthermore, the seasonal forcing over the Indian Ocean can penetrate into the second layer of the model, which is about 275 m deep, resulting in an annual amplitude of 5 cm s^{-1} for the maximum northward

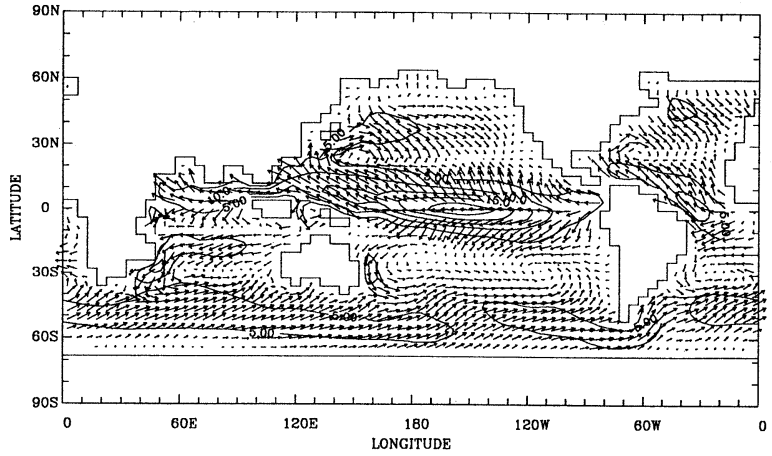

Fig. 10a. Simulated monthly mean surface layer current with isopleths of current speeds (cm s^{-1}) in January.

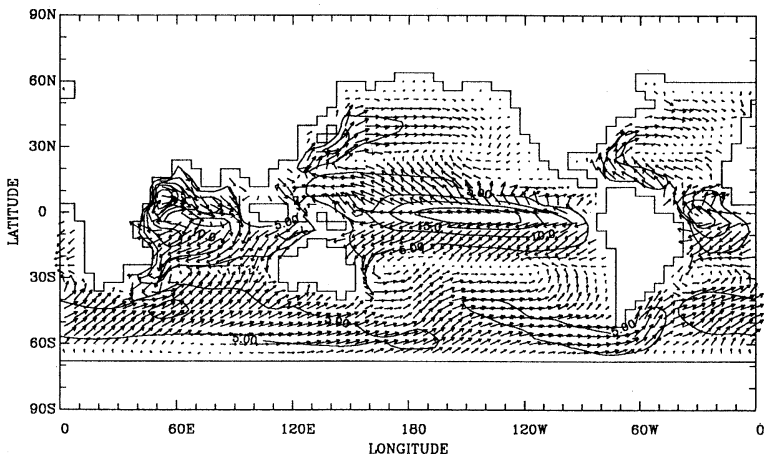

Fig. 10b. Simulated monthly mean surface layer current with isopleths of current speeds (cm s^{-1}) in July.

current in the subsurface layer (Fig. 11a). On the other hand, no significant signal of seasonal variability in the subsurface layer has been found in the other basins.

Acknowledgements

We thank Miss Xuan WANG for assistance in preparing the manuscript and figures and Dr. Zhuo LIU for proofreading the text. We also thank the reviewers for their helpful comments, many of which are incorporated in the final text.

This work was supported by the National Natural Science Foundation and the Academia Sinica of the People's Republic of China.

Reference

ARAKAWA, A. and V.R. LAMB (1977): Computational desigin of the basic dynamical processes of UCLA general circulation model. *In* Methods in Computational Physics, Vol. 17, General Circulation Models of the Atmosphere, J. CHANG (Ed.), Academic Press, New York, 173–265.

BAO, N. and X.H. ZHANG (1991): Effect of ocean thermal diffusivity on global warming induced by increasing atmospheric CO_2. Adv. Atmos. Sci., **8**, 421–430.

BATTEEN, M. and Y.-J. HAN (1981): On the computational noise of finite-difference schemes used in ocean models. Tellus, **33**, 387–396.

BRYAN, F. (1987): Parameter sensitivity of primitive equation ocean general circulation

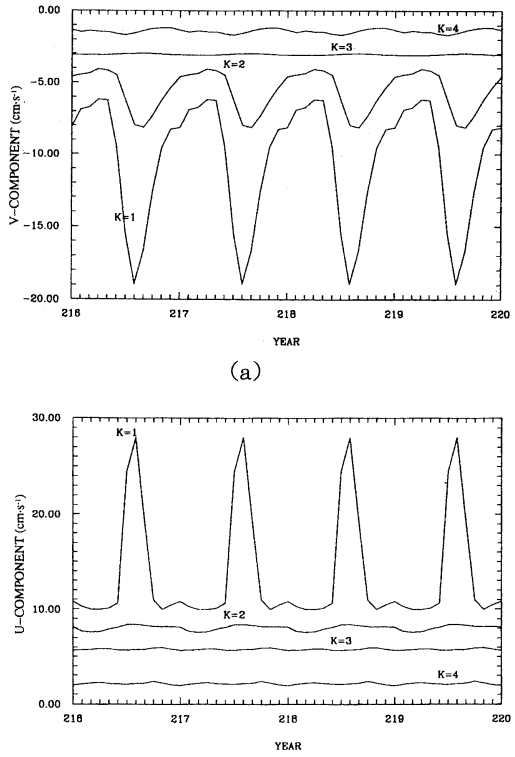

Fig. 11. Simulated seasonal variation of maximum northward currents (a) and maximum eastward currents (b) in the Indian Ocean (cm s^{-1}).
K=1 - surface layer (−2.0 for v and +1.0 for u);
K=2 - second layer (−3.0 for v and +2.0 for u);
K=3 - third layer (−2.0 for v and +3.0 for u);
K=4 - bottom layer (−0.5 for v and +1.0 for u).

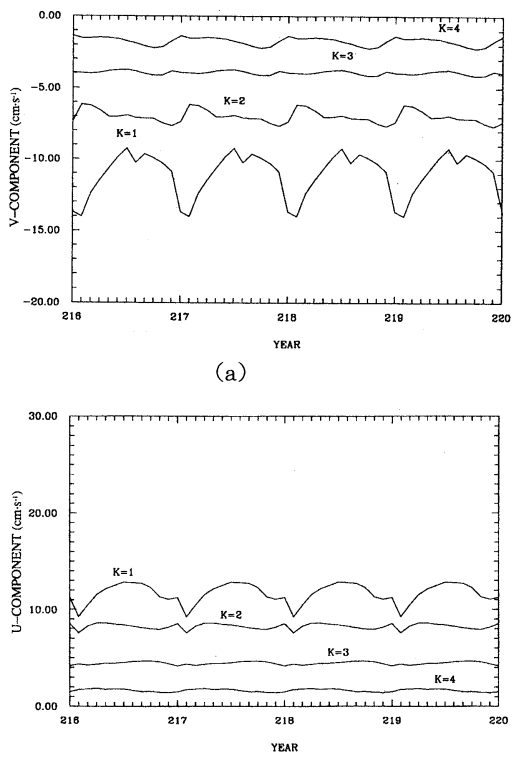

Fig. 12. Simulated seasonal variation of maximum northward currents (a) and maximum eastward current (b) in the North Pacific (cm s^{-1}).
K=1 - surface layer (−0.0 for v and +2.0 for u);
K=2 - second layer (−1.5 for v and +2.0 for u);
K=3 - third layer (−3.0 for v and +3.0 for u);
K=4 - bottom layer (−1.0 for v and +1.0 for u).

models. J. Phys. Oceanogr., **17**, 970–985.

BRYAN, K. and M. COX (1972): An approximate equation of state for numerical models of ocean circulation. J. Phys. Oceanogr., **2**, 510–514.

BRYAN, K. and L.J. LEWIS (1979): A water mass model of the world ocean. J. Geophys. Res., **84**, 2503–2517.

ECKART, C. (1958): Properties of water. Part II. Am. J. Sci., **256**, 225–240.

ESBENSEN, S.K. and Y. KUSHNIR (1981): Heat budget of the global ocean: Estimates from surface marine observations. Report 29, Climatic Resarch Institute, Oregon State University, Corvallis, Oregon, 271 pp.

HAN, Y.-J. (1984): A numerical world ocean general circulation model. Part I : Basic design and barotropic experiment. Part II : A baroclinic experiment. Dyn. Atmos. and Oceans, **8**, 107–172.

HAN, Y.-J. and S.-W. LEE (1981): A new analysis of monthly mean wind stress over the global ocean. Report 26, Climatic Research Institute, Oregon State University, Corvallis, Oregon, 148 pp.

LEVITUS, S. (1982): Climatological Atlas of the World Ocean. NOAA Professional Paper 13, U.S Government Printing Office, Washington, D. C., 173 pp.

MUNK, W.H. (1966): Abyssal recipes. Deep-Sea Res., **13**, 707–730.

ROOTH, C.G. and H.G. OSTLUND (1972):Penetration of tritium into the Atlantic thermocline. Deep-Sea Res., **19**, 481–492.

WYRTKI, K. (1974): The dynamic topography of the Pacific Ocean and its fluctuations. Report

H-16-74-S. Hawaii Inst. Geophy., 19 pp.

ZENG, Q.C. (1983): Some numerical ocean-atmosphere coupling models. First International Symp. Integrated Global Ocean Monitoring. Tallinn, USSR.

ZENG, Q.C. and X.H. ZHANG (1987): Available energy conservation schemes for primitive equations of spherical baroclinic atmosphere. Chin. J. Atmos. Sci., **11**, 121–142.

ZENG, Q.C., X.H. ZHANG and R.H. ZHANG (1991): A design of an oceanic GCM without the rigid lid approximation and its application to the numerical simulation of the circulation of the Pacific Ocean. J. Mar. Systems, **1**, 271–292.

ZENG, Q.C., Z.Z. JI and C.G. YUAN (1982): Design of difference schemes for primitive equations. Scientia Sinica, Series B, XXV(2), 183–199.

ZHANG, X.H. and N. BAO (1990) : Buoyancy equation and salinity computation. Annual Report 1989, Laboratory of Atmospheric Sciences and Geophysical Fluid Dynamics, Institute of Atmospheric Physics, Academia Sinica, 193–203.

ZHANG, X.H. and Q.C. ZENG (1988): Computational desigin of world ocean general circulation model. Chin. J. Atmos. Sci., special issue, 149–165.

ZHANG, X.H. and X.Z. LIANG (1989): A numerical world ocean general circulation model. Adv. Atmos. Sci., **6**, 44–61.